Steel and Composite Structures, Vol. 10, No. 5 (2010) 429-455
DOI: http://dx.doi.org/10.12989/scs.2010.10.5.429

Air blast load generation for simulating structural response

Emily L. Guzas* and Christopher J. Earls

School of Civil and Env. Eng., Cornell University, Ithaca, NY, USA

(Received December 12, 2009, Accepted August 19, 2010)

Abstract. The current research presents a detailed methodology for generating air blast loading for use within a finite element context. Parameters describing blast overpressure loading on a structure are drawn from open literature sources and incorporated within a blast load generation computer code developed for this research. This open literature approach lends transparency to the details of the blast load modeling, as compared with many commonly used approaches to blast load generation, for which the details are not publicly available. As a demonstration, the load generation code is used with the finite element software LS-DYNA to simulate the response of a steel plate and girder subjected to explosions modeled using these parameters as well as blast parameters from other sources.

Keywords: air blast; extreme loading; explosion; blast load modeling; nonlinear finite element analysis.

1 Introduction

In recent years, human threat to structures has become highlighted as a concern worldwide. The results of terrorist attacks have demonstrated that conventionally designed structures are vulnerable to explosive loading, with localized blast damage initiating global collapse in some cases (Corley 2004). As it is that this particular scenario is outside of the realm of common practice for structural engineers, it is important that an understanding of the unique loading features of the hazard be considered. Along these lines, a transparent means for generating analogs to air blast loading of structures is a required point of departure supporting this outcome.

1.1 Overview

Air blast, which involves the detonation of explosive material in air, can be modeled with a decaying exponential equation form that uses a series of parameters, which depend on explosive charge size, type, and distance to a target. There are numerous different sets of air blast parameter data available in the literature, both in graphical and equation forms (Baker 1973, Baker *et al*. 1983, Kinney and Graham 1985, Kingery and Bulmash 1984, Smith and Hetherington 1994). However, the data provided in these sources varies in terms of usability and completeness, as discussed in detail in a separate section of this paper.

Thus, one of the objectives of the research presented herein is to provide a complete set of blast parameter definitions from the open literature and to implement these in a load generation code to produce air blast loading for finite element simulations of structures subjected to explosive air burst. By

* Corresponding author, Ph.D., E-mail: ecl38@cornell.edu

employing open literature sources only, the designer is able to investigate all assumptions in the load generation process, something that is not possible when using load generation software that is restricted in usage and distribution. The air blast load generation code developed for this research is capable of applying spatially and temporally varying blast loads to a structure. Improvements on a previously published approach for air blast load generation by Chock and Kapania (2001) are the inclusion of angle of incidence and shielding effects, and the use of equation forms for parameters rather than relying on tabular data.

Also, since there exist numerous disparate collections of air blast parameter data, a second goal of this research is to compare structural responses corresponding to different sets of parameter data, where the blast loading is applied to the test problems using the developed blast load generation code. The intent here is to examine any difference in response as a result of relatively small, but legitimate, changes in parameter definition.

1.2 Literature review

There is a variety of previous research regarding different air blast modeling approaches and uncertainty in explosive air burst. Beshara (1994) drew on sources in the unclassified literature to review numerous aspects of external blast load modeling on aboveground structures, including equations for various parameters. Beshara pointed out that structural response depends on numerous blast loading parameters, all of which are difficult to define with any certainty.

Santiago and Bhattacharya (1991) investigated the response of an aluminum plate to an air blast, where the loading is based on an uncoupled hydrocode calculation of a shock wave.

The hydrocode results were sampled at different spatial intervals, producing loading functions varying widely in terms of peak overpressure, impulse, and arrival time. Their results showed that the plate response is most sensitive to an impulse parameter.

Chock and Kapania (2001) provided an in-depth review of air blast phenomenology, and compared the air blast loading approaches used by Baker (1973) versus Kingery and Bulmash (1984). They also developed an air blast load generation code based on the graphical results of Baker and the equations of Kingery and Bulmash. They compared a blast overpressure profile for one explosion scenario, and evaluated the structural response of an arbitrary aircraft wing subjected to an explosion modeled using the Kingery-Bulmash equations.

Bogosian *et al*. (2002) compared air blast loading produced by three major blast generation programs, ConWep, SHOCK, and BlastX, all of which are restricted to use by the U.S. military and government contractors. They focused on the parameters of reflected positive phase overpressure, positive incident overpressure, positive incident impulse, as well as a few negative phase parameters. They developed a database of experimental explosives data for a wide variety of explosion sizes, charge materials and shapes, and blast scenarios, covering a range of scaled distances from $1.2 - 40$ m/kg$^{1/3}$. Their statistical analysis indicated that the two-sigma range of parameter values was 1/3 to 2/3, a very large range.

Baylot and Rickman (2007) followed up on the work of Bogosian *et al*. (2002) with an investigation of the uncertainty in air blast overpressures and impulses, as measured experimentally. They carried out small scale (1 : 50) experiments of a nine-building arrangement simulating an urban setting, where data were taken from a number of pressure transducers located on the different buildings. When comparing anywhere from 4–11 measurements of the same parameters for nominally identical charge sizes and standoff distances, they found that the maximum values for a parameter deviated from 15% to 90% above the averaged value for a test.

Florek and Benaroya (2005) reviewed research on air blast load modeling approaches and their effects on structural deflections, especially with regard to aviation structures. They focused on the analysis of beams, plates, shells, and single degree of freedom (SDOF) systems as representative structures subjected to pulse loading of a variety of shapes, from triangular to square to decaying exponential. In particular, they discussed attempts to eliminate pulse shape effects in rigid plastic materials.

Borenstein and Benaroya (2009) examined the response of a clamped aluminum plate to a simulated blast loading employing a decaying exponential form, with either an instantaneous rise or a finite rise to a peak overpressure level. The rectangular plate was modeled as an elastic-perfectly plastic material, with the plasticity modeled via plastic yield lines in a standard envelope pattern. In order to create samples of loading for a Monte Carlo analysis, they assumed that one (or sometimes all) of the loading parameters was a uniformly distributed random variable, with any remaining variables (determined from Kingery and Bulmash (1984)) left deterministic. Their sensitivity study determined that, in the majority of cases, the structural response was most sensitive to load duration time.

The current work builds upon previous research in numerous aspects. First, it provides a omplete set of parameter equations from the open literature, drawn from Kinney and Graham (1985) and Brode (1977). These open air literature sources are vital for analysts needing to understand the assumptions inherent within the loading model, thus avoiding a "black box" condition. Also, this research compares structural responses for a plate and a girder subjected to loading modeled with these parameters, with the well-known Kingery-Bulmash parameters, and also with equivalent triangular pulse loading. These example problems demonstrate the code capability when used as a preprocessor to generate loading for nonlinear finite element analyses carried out using commercial software.

1.3 Paper organization

Background on air blast phenomenology is given in Section 2 of the current paper, while Section 3 includes information about air blast parameters (including the proposed parameter equations) and discusses the development of the air blast load generation code. Section 4 presents the case studies examined for this research: a plate and a girder subjected to various air blast loadings. Case study results are presented in Section 5 and conclusions are drawn in Section 6.

2. Air blast phenomenology

2.1 Air blast overpressures

The evolution of an air blast involves various stages: detonation, shock wave formation and propagation, and a decay in the shock wave strength that ends with a return to ambient conditions. In the context of this research, air blast refers to the detonation of a conventional high explosive, such as Trinitrotoluene (TNT), in air.

Following detonation, an explosive air burst arises out of a rapid expansion of gases that initiates a shock wave. The shock wave propagates radially outwards from the detonation epicenter. At the shock wave front there is a sharp discontinuity in air pressure, to a peak level above atmospheric conditions (peak overpressure), representing the compression of the air medium. Fig. 1 shows a schematic of a typical time history of overpressure at a stationary location affected by an explosion in air. This overpressure time history, or air blast profile, consists of a positive phase and a negative (suction) phase. In many

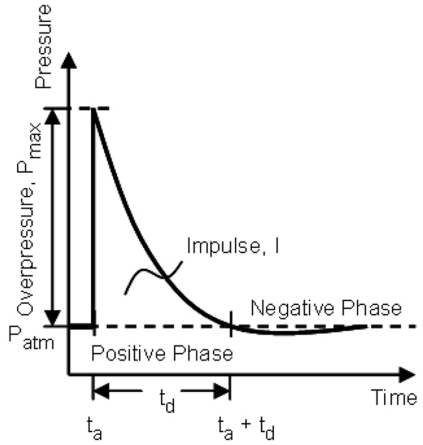

Fig. 1 Schematic of a typical open air blast profile

cases, the negative phase of the blast overpressure time history can be ignored for structures, especially those without an abundance of frangible materials (Baker *et al*. 1983).

Any structure or object in the path of the shock wave will reflect the wave. The obstruction of the air velocity at the structure surface induces a significant increase in load on the structure.

Thus, when describing the loading on a structure induced by explosive air burst, reflected and side-on (free air) cases are treated separately, with different values for reflected peak overpressure and side-on peak overpressure.

At a stationary point in space, the effects of air blast have frequently been modeled with a modified Friedlander's equation (Borenstein and Benaroya 2009), as

$$P(t) = \begin{cases} 0, & t < t_a, \\ P_{max}\left(1 - \dfrac{t - t_a}{t_d}\right) e^{-b\left(\frac{t-t_a}{t_d}\right)}, & t_a \le t \le t_a + t_d, \\ 0, & t > t_a + t_d, \end{cases} \tag{1}$$

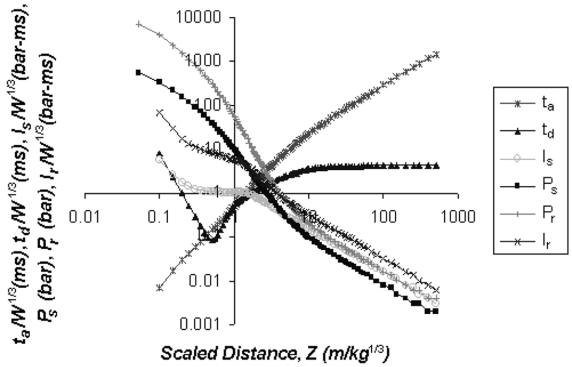

Fig. 2 Scaled blast load parameters used in air blast loading program

where $P(t)$ is the overpressure at time t after detonation, P_{max} is the peak overpressure, t_a is the arrival time of the shock wave, t_d is the duration of the shock wave, and b is the decay constant. Depending on whether or not the point of interest is located on the surface of an object, P_{max} is either equal to P_s, the peak side-on overpressure (in free air) or P_r, the maximum reflected overpressure (upon shock wave reflection at a rigid surface).

2.2 Blast scaling

In empirical approaches, air blast parameters are most often presented for a reference explosion, and some type of scaling is subsequently used to obtain the parameter values for the actual charge weight of interest (Baker 1973, Baker *et al*. 1983, Kinney and Graham 1985, Smith and Hetherington 1994). The two types of scaling most commonly used are Sach's scaling and Hopkinson scaling (Baker 1973, Baker *et al*. 1983, Kinney and Graham 1985). Sach's scaling is a more generic form of Hopkinson scaling that is especially suited for predicting characteristics of blast waves from explosive bursts at high altitudes, such as nuclear bomb detonations (Baker *et al*. 1983). Since the current research is focused on detonations of conventional high explosives, instead of nuclear materials, Hopkinson scaling is appropriate.

The Hopkinson scaling law states that when two charges of the same explosive material are detonated in the same atmospheric conditions, similar shock wave effects are experienced at equivalent scaled distances, Z, defined as

$$Z = \frac{R}{W^{1/3}}, \tag{2}$$

where R is the standoff distance, or distance between a point of interest and the blast epicenter, and W is the charge weight. In the literature, various parameters quantifying the effects of explosive air burst are

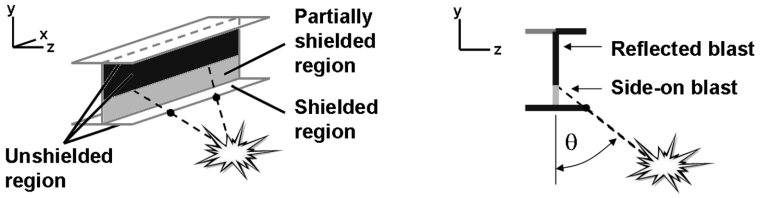

Fig. 3 Schematic of shielding effects included in air blast loading program

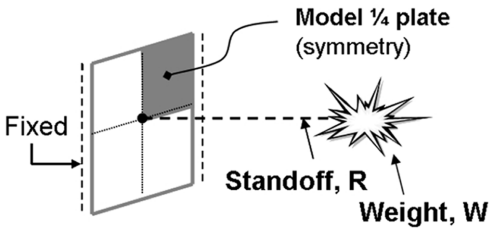

Fig. 4 Plate model set-up

defined as a function of scaled distance, Z, for a reference explosion. This reference explosion almost always corresponds to a charge weight equal to either 1 kg or 1 lb of TNT.

For explosives other than TNT, the usual approach is to calculate an equivalent weight in TNT for the explosive, W_{TNT}, according to

$$W_{TNT} = \frac{H_{exp}}{H_{TNT}} w_{exp}, \tag{3}$$

where w_{exp} is the weight of the explosive, and H_{exp} and H_{TNT} are the heats of detonation for the explosive and for TNT, respectively (Beshara 1994). In some sources, the ratio H_{exp} / H_{TNT}, which represents the ratio of energy output between a given explosive and TNT, is called the TNT equivalence factor. Values for the heat of detonation for more common explosives are tabulated in Kinney and Graham (1985) and Baker *et al*. (1983).

Hopkinson scaling assumes that pressures, temperatures, densities, and velocities are the same at homologous times. Parameter data from the literature, as applied to a given explosion, are then determined by applying a scaling factor to parameter values for a reference explosion at the same scaled distance. The scaling factor is unity for peak overpressures, but times and impulses are scaled by the factor $k = (W/W_{ref})^{1/3}$, where W is the weight (equivalent TNT) of the charge of interest and W_{ref} is the weight of the reference explosion.

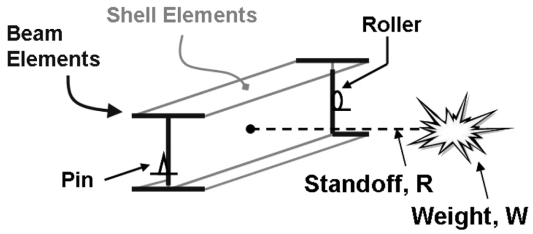

Fig. 5 Girder model set-up

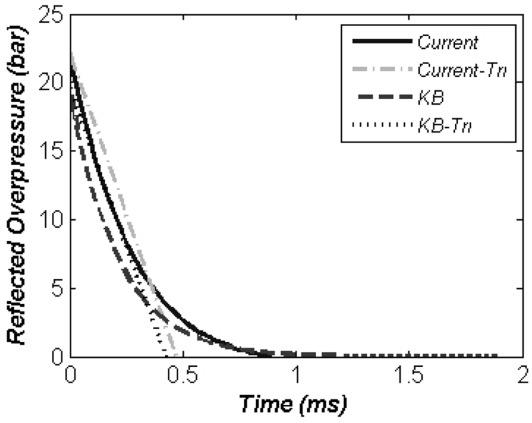

Fig. 6 Comparison of overpressure profiles for $R = 1.52$ m, $W = 1.36$ kg

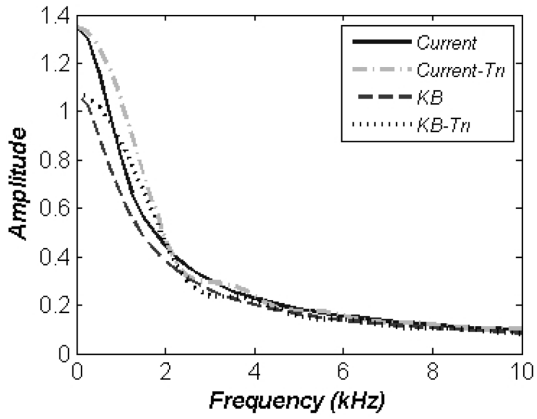

Fig. 7 Comparison of frequency content of air blast loading for R = 1.52 m, W = 1.36 kg.

3. Air blast load generation code

The air blast load generation computer code written as part of the current research determines overpressure profiles at nodal locations within a finite element model for a given explosion scenario. The overpressure time histories are calculated based on Eq. (1), and are converted to nodal force time histories using element tributary area. The associated air blast parameters are calculated as a function of scaled distance, angle of incidence, and charge type (spherical or hemispherical). A choice of different blast parameter sources is available for the air blast load computation.

3.1 Blast parameters

Values for the parameters describing air blast in Eq. (1) can be found in a few different sources. The work of Baker (Baker 1973, Baker *et al*. 1983) is very thorough, including information about both reflected and side-on air blast cases, but the graphical format of the data is not very conducive to implementation within an air blast loading code. The work of Kingery and Bulmash (1984) includes blast data from numerous different tests, both for side-on and reflected cases, and their data is presented in the form of equations as a function of scaled distance. These air blast parameter equations (known as

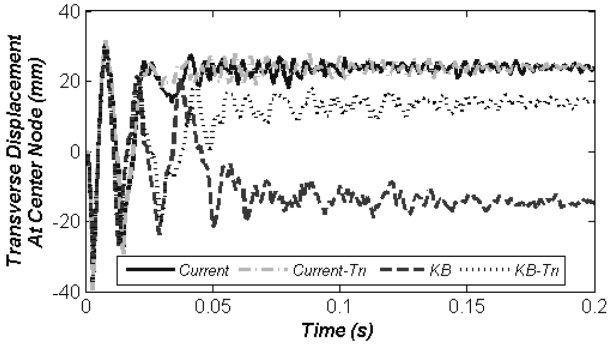

Fig. 8 Comparison of plate transverse displacement at center

the Kingery-Bulmash equations) serve as the basis for ConWep (Hyde 1992), which is a well-known air blast load generation program. However, it is important to note that both ConWep and the work of Kingery and Bulmash are limited in distribution, only available to the U.S. military and government contractors. Other works(Smith and Hetherington 1994, Kinney and Graham 1985) include alternative equations for air blast parameters, but do not include complete information, especially regarding reflected air blast. Baker *et al*. (1983) includes detailed information about peak values of shock overpressure, as taken from Brode (1977).

3.1.1 Blast parameters following Kinney and Graham and Brode

The air blast parameter equations presented in this section comprise a complete set of parameter equations from open literature sources. The equations are taken from Kinney and Graham (1985) and Brode (1977), with some modifications and additions.

The duration time, taken directly from Kinney and Graham (1985), is given as

$$\frac{t_d}{W^{1/3}} = \frac{980\left[1+\left(\frac{z}{0.54}\right)^{10}\right]}{\left[1+\left(\frac{z}{0.02}\right)^{3}\right]\left[1+\left(\frac{z}{0.74}\right)^{6}\right]\sqrt{1+\left(\frac{z}{6.9}\right)^{2}}}, \tag{4}$$

where t_d is the duration, in seconds, of the positive phase of the blast profile.

Information about the peak overpressure in free air is also taken directly from Kinney and Graham (1985), and is defined as

$$P_s = 808P_{atm}\frac{\left[1+\left(\frac{z}{4.5}\right)^{2}\right]}{\sqrt{\left[1+\left(\frac{z}{0.048}\right)^{2}\right]\left[1+\left(\frac{z}{0.32}\right)^{2}\right]\left[1+\left(\frac{z}{1.35}\right)^{2}\right]}}, \tag{5}$$

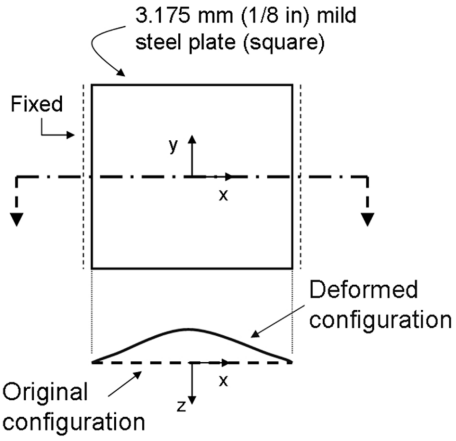

Fig. 9 Schematic of plate center displacement profile

where P_s is the peak side-on overpressure in units of bars, and P_{atm} is the atmospheric pressure in bars.

As part of the development of an experimental air blast database, Bogosian *et al*. (2002) tabulated the distribution of blast test data points available for reflected and incident blast parameters. This summary indicated a similar number of available data sets for reflected and for incident overpressure measurements; however, information regarding peak reflected overpressure, P_r, is much harder to find than for incident overpressure in the open literature. All sources that do include parameter information for reflected overpressures present data for the normally reflected case, with angle of incidence effects treated separately, if at all.

In the far field limit for explosions of any size, or for small explosions, the air can be treated as an ideal gas in order to establish a relationship between the peak side-on overpressure and peak reflected overpressure at a surface. According to Brode (1977), this relationship is

$$P_r = P_s\left(2+\frac{6P_s}{P_s+7P_{atm}}\right), P_s < 6.9\text{bar} \tag{6}$$

where P_r is the maximum overpressure for normal reflection, P_s is the peak side-on overpressure, and P_{atm} is the ambient air pressure. An implicit assumption in this equation is that $\gamma = 1.4$, where γ is the heat capacity ratio of the air medium.

When overpressure values exceed 6.9 bar, molecules in the air start to interact with one another and

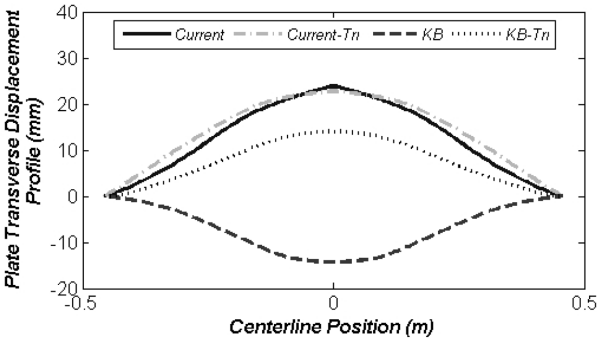

Fig. 10 Comparison of plate center displacement profiles at $t = 200$ ms

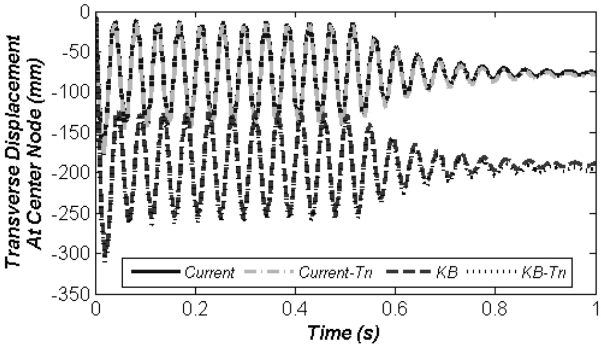

Fig. 11 Comparison of girder transverse displacement at mid-height, mid-span

the ideal gas assumption is no longer valid. For this regime, Brode (1977) defines the peak normally reflected overpressure as

$$P_r = P_s\left(\frac{0.03851P_s}{1+0.0025061\ P_s+4.041\times10^{-7}P_s^2}+2+\frac{0.004218+0.7011\ P_s+0.001442\ P_s^{\ 2}}{1+0.1160\ P_s+8.086\times10^{-4}P_s^2}\right),\ P_s\geq 6.9\text{bar}, \tag{7}$$

where P_s is again the peak side-on overpressure in bars.

Suitable expressions for the decay constant and the arrival time are not included in the works of Kinney and Graham (1985) or Brode (1977). Thus, the following equations for arrival time and decay constant are developed by fitting piecewise polynomials to data for a 1 kg TNT reference explosion in Kinney and Graham (1985). The data include arrival times and decay coefficients over a range of scaled distances.

The resulting expression for the arrival time is

$$\frac{t_a}{W^{1/3}} = \sum_{i=1}^{4} a_i Z^{i-1}, 0.3\leq Z\leq 500\ \text{m/kg}^{1/3}, \tag{8}$$

where t_a is the arrival time, in seconds, of the shock wave initiated by an air blast. Values for the fitted polynomial coefficients, a_i, are included in Table 1 for various ranges of Z.

A higher order of polynomial is required to produce an accurate fit for the decay constant over the range of scaled distances, especially for smaller scaled distances. The decay constant follows this relationship

$$b = \sum_{i=1}^{6} c_i Z^{i-1}, 0.3\leq Z\leq 500\ \text{m/kg}^{1/3}, \tag{9}$$

where b is the dimensionless decay constant for side-on air blast. Values for the fitted polynomial coefficients, c_i, are shown for different ranges of Z in Table 2.

The decay constant is determined from the positive phase impulse, or the area under the pressure time history curve, for either side-on or reflected blast. Kinney and Graham (1985) tabulate the decay constant for a wide range of distances, but only for side-on blast. By assuming similarity between time histories of side-on overpressure and normally reflected overpressure, demonstrated by

$$\frac{I_r}{I_s} = \frac{P_r}{P_s}, \tag{10}$$

Table 1 Fitted polynomial coefficients to define the arrival time

Range (m/kg$^{1/3}$)	a_0	a_1	a_2	a_3
0.3 ≤ Z < 2.4	1.769362e − 2	−2.032568e − 2	5.395856e − 1	−3.010011e − 2
2.4 ≤ Z < 12	−2.251241e + 0	1.765820e + 0	1.140477e − 1	−4.066734e − 3
12 ≤ Z ≤ 500	−6.852501e + 0	2.907447e + 0	9.466282e − 5	−9.344539e − 8

Table 2 Fitted polynomial coefficients to define the decay coefficient

Range (m/kg1/3)	c_0	c_1	c_2	c_3	c_4	c_5
$0.3 \le Z < 0.95$	3.08473e + 2	–2.14692e + 3	5.95329e + 3	–8.22603e + 3	5.68743e + 3	–1.57341e + 3
$0.95 \le Z < 2.4$	1.76074e + 1	–2.67855e + 1	1.78607e + 1	–5.65557e + 0	6.94164e – 1	0
$2.4 \le Z < 6.5$	4.43216e + 0	–2.71877e + 0	7.41973e – 1	–9.34132e – 2	4.46971e – 3	0
$6.5 \le Z < 40$	7.11610e – 1	–6.26846e – 2	3.32532e – 3	–8.24049e – 5	7.61887e – 7	0
$40 \le Z \le 500$	2.51614e – 1	–1.76758e – 3	9.51638e – 6	–2.19712e – 8	1.79135e – 11	0

the decay constant can be used interchangeably for side-on and normally reflected cases (Baker *et al*. 1983). While this assumption may introduce error into the prediction of I_r, Baker (1973) includes plots of reflected impulse measured experimentally over a wide range of scaled distances, with confidence intervals, and these plots shows that there is an extremely wide range of data for reflected impulse. Considering that there is a lack of reflected data in the literature, the authors determined that the assumption of similarity was an acceptable one.

The above parameter equations for ta and b are evaluated for goodness-of-fit by using the following error metric based on a normalized ℓ_2 norm,

Fig. 12 Contours of accumulated effective plastic strain at $t = 1$ s

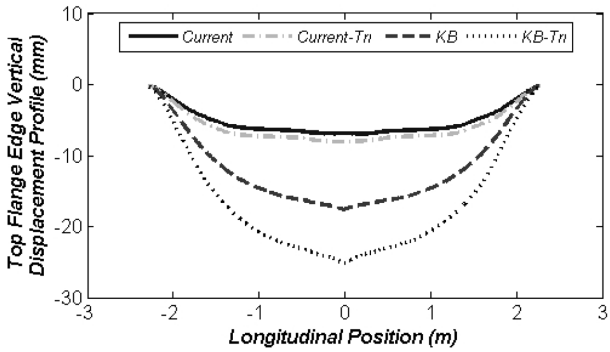

Fig. 13 Comparison of girder flange edge displacement profile at $t = 1$ s

$$Error = \frac{\|x - x_{dat}\|_2}{\|x_{dat}\|_2} = \frac{\sqrt{\sum_{i=1}^{N}[(x)_i - (x_{dat})_i]^2}}{\sqrt{\sum_{i=1}^{N}[(x_{dat})_i]^2}}, \tag{11}$$

where (x)i is the parameter value calculated at scaled distance Z_i using the appropriate parameter equation, $(x_{dat})i$ is the corresponding parameter value tabulated in Kinney and Graham (1985), and N is the total number of scaled distances included in the tabulated data. Error values for each of the parameter equations, as calculated with Eq. (11), are 6.63×10^{-4} for P_s, 4.85×10^{-7} for t_d, 3.18×10^{-7} for t_a, and 4.21×10^{-4} for b.

Since similarity has been assumed in air blast profiles for reflected and side-on cases, via Eq. (10), then the impulse can be calculated by integrating $P(t)$ in Eq. (1) to get the expression

$$I = \frac{P_{max} t_d e^{-b}(be^b - e^b + 1)}{b^2} \tag{12}$$

where I is either the reflected or side-on impulse, P_{max} is either the reflected or side-on peak overpressure, t_d is the duration time, and b is the decay constant. Upon investigation, fitting the decay constant according to Eq. (9) actually provides a better approximation to the sideon impulse data in Kinney and Graham (1985), as compared with the equation Kinney and Graham developed from the same data set for side-on impulse,

$$I_s = \frac{0.067\sqrt{1 + \left(\frac{z}{0.23}\right)^4}}{Z^2\sqrt[3]{1 + \left(\frac{z}{1.55}\right)^3}} \tag{13}$$

The relative error for calculated I_s values, as compared to the corresponding tabulated data in Kinney and Graham (1985), is 3.06×10^{-2} for Is from Kinney and Graham, Eq. (13), and is 1.89×10^{-4} using the fitted equation for b to calculate I_s, Eq. (12). Besides the increase in accuracy as compared to tabulated data, using a parameter equation for the decay constant, rather than impulse, is advantageous because this avoids the need for root-solving to calculate the decay constant for each overpressure time history generated by the air blast loading code.

The blast parameter values over a range of scaled distances are summarized in Fig. 14. The decay constants are not shown in this figure, but rather are used to calculate values for side-on impulse, I_s, and reflected impulse, I_r, according to Eq. (12), for various scaled distances.

3.1.2 Blast parameters from Kingery and Bulmash

The approach by Kingery and Bulmash (1984) involves numerically fitting functions to data from various explosive tests. The resulting Kingery-Bulmash equations are defined in terms of log-log scaling, and take the form of

$$Y = C_0 + C_1 U + \ldots + C_N U^N \tag{14}$$

where

$$U = K_0 + K_1 T. \tag{15}$$

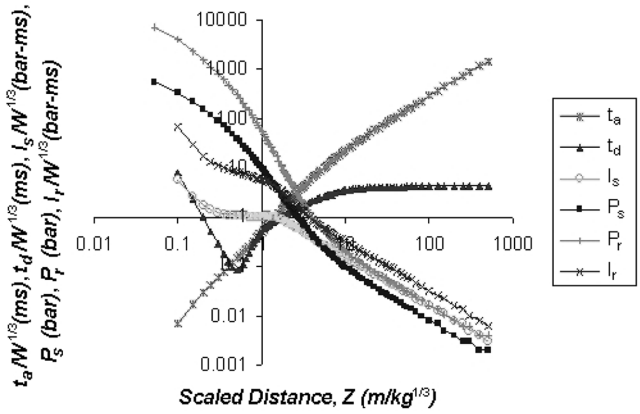

Fig. 14 Scaled blast load parameters used in air blast loading program

In these equations, Y is the common logarithm of the blast parameter of interest (*e.g.*, P_r or $t_d / W^{1/3}$), T is the base 10 logarithm of the scaled distance, Z, and N is the order of fit. Values for the coefficients C and K are not available within the open literature. Thus, while the Kingery-Bulmash equations are widely used by the U.S. military and government contractors, they are not available for research publishable in the open literature.

3.1.3 Blast parameters for design

Numerous sources including military technical manuals, such as *TM 5-1300* (US Army 1990), and other sources on design (Smith and Hetherington 1994) suggest a simplification to the decaying exponential blast profile shown in Fig. 1. This approach involves approximating the typical overpressure profile with an equivalent triangular pulse. The peak overpressure, P_{max}, and the impulse, I, are preserved but the duration time is modified as

$$t_d' = \frac{2I}{P_{max}} \tag{16}$$

The decay constant, b, is set to zero to give a triangular shape to the blast profile.

Accordingly, the equivalent triangle assumption can be applied to either the currently proposed set of parameter equations (following Kinney and Graham (1985) and Brode (1977)) or the Kingery-Bulmash equations (Kingery and Bulmash 1984), for use in the air blast load generation code developed for this research.

3.2 Angle of incidence

The angle at which a shock wave strikes a structure affects the magnitude of the peak reflected blast overpressure. In fact, there is a complex relationship between the coefficient of reflection, C_r, which is a ratio of the peak reflected overpressure to the peak side-on overpressure, and the angle of incidence, θ. As discussed by Chock and Kapania (2001), assuming normal reflection is conservative and easier to implement within a blast generation program. However, Randers-Pehrson and Bannister (1997) account for angle of incidence effects in their implementation of ConWep into DYNA2D and DYNA3D, an

implementation that carries over into the commercial LS-DYNA.

Within their implementation, the reflected blast overpressure profile is a function of both time and angle of incidence and it is a combination of the normally reflected and side-on blast overpressure time histories. Accordingly, the air blast profile, $P(t, \theta)$, to be applied to an individual finite element at a point in time is calculated as

$$P(t,\theta) = P_r(t)cos^2\theta + P_s(t)(1+cos^2\theta - 2cos\theta), \tag{17}$$

where θ represents the angle between the normal of an element surface, which includes the point of interest, and a ray between the point of interest and the blast detonation point. $P_r(t)$ is the reflected air blast profile, following Eq. (1) with $P_{max} = P_r$, and $P_s(t)$ is the side-on blast profile, which is computed from Eq. (1) with $P_{max} = P_s$. To ensure proper air blast load calculation using Eq. (17), element normals must point toward (instead of away from) the blast source.

For all of the loading options implemented within the air blast load generation code, the incident impulse is calculated as

$$I(\theta) = I_r cos^2\theta + I_s(1+cos^2\theta - 2cos\theta), \tag{18}$$

where I_r is the impulse for normal reflection, I_s is the side-on impulse, and θ is the angle of incidence. The duration time for the equivalent triangular parameter equations is a function of this incident impulse,

$$t_d'(\theta) = \frac{2I(\theta)}{P(t=t_a,\theta)} = \frac{2I(\theta)}{P_r cos^2\theta + P_s(1+cos^2\theta - 2cos\theta)}, \tag{19}$$

where $P(t = t_a, \theta)$ is the overpressure at the arrival time, from Eq. (17), P_r is the peak reflected overpressure for normal incidence, and P_s is the peak side-on overpressure.

However, for the loading approach using the proposed equations, the assumption of similarity in Eq. (10) simplifies the incorporation of angle of incidence effects within the developed air blast load generation code. Since $P_r / I_r = P_s / I_s$ and the decay constant is the same for both reflected and side-on air blast, then the incident overpressure time history for the proposed equations can be calculated using the modified Friedlander equation in Eq. (1), with

$$P_{max}(\theta) = P_r cos^2\theta + P_s(1+cos^2\theta - 2cos\theta), \tag{20}$$

where θ is the angle of incidence, P_r is the peak overpressure for normal reflection, and P_s is the maximum side-on overpressure.

Currently the air blast load generation code employed herein uses the same methodology for estimating angle of incidence effects as the implementation of ConWep in LS-DYNA, from Randers-Pehrson and Bannister (1997). Future work could focus on improving the calculation of P_{max} to account for the Mach stem effect, which is not accounted for in (Randers-Pehrson and Bannister 1997).

3.3 Hemispherical blast

Explosions located at the ground surface are categorized as hemispherical blast. In *TM 5-1300*, there

are separate sets of parameters for spherical and hemispherical blast (US Army 1990). However, these parameters are presented in graphical form and were drawn from sources not available in the open literature. Thus, for the current research the magnification factor approach (Baker 1973, Kingery and Bulmash 1984, Smith and Hetherington 1994) described subsequently has been employed.

When a charge is detonated at the ground surface, simultaneous reflected waves from the ground are produced, reinforcing the shock wave generated by the initial explosion. If the ground were a perfect reflecting surface, this magnification effect would be equivalent to the shock produced by a charge twice the weight of the actual explosive. However, experimental data indicate that the magnification factor should be less than two (but more than one) because the ground absorbs energy for surface bursts. In fact, a magnification factor of 1.8 is suggested by multiple sources (Baker 1973, Kingery and Bulmash 1984, Smith and Hetherington 1994), and is employed within the air blast load generation code developed for this research. Accordingly, the approach for hemispherical blast is exactly the same as for spherical blast, except that the charge weight W is replaced by 1.8W.

3.4 Shielding effects

For explosive air burst on structures with more complex geometries than a single flat surface, shielding and wave diffraction affect the applied load distribution. Shielding is a function of component geometry and blast location. In this research, shielding effects are incorporated into the blast load generation code using a ray tracing technique to determine which surfaces of a structure are in direct line of sight to an explosion.

Accordingly, fully reflected air blast loads are applied to regions with an unobstructed path from detonation source point to structural boundary. However, in regions of a structural surface that are not in direct line of sight to an explosion, the loading situation is much more complex, especially in the vicinity of sharp corners (Bleakney *et al*. 1950). Shock waves diffract around corners, and so while the air is compressed above atmospheric pressure at the surface beyond a corner, the overpressure here does not reach fully reflected levels. Applying fully reflected loading to this region would be very conservative, although not applying any loading at all would not be representative of the physical situation. Thus, in areas of a surface partially shielded by another part of the structure, the air blast load generation code models the magnification of the surrounding overpressure with an applied blast loading corresponding to the side-on, or free air, overpressure.

As an example, Fig. 15 illustrates a wide flange member subjected to an explosion where the bottom flanges partially shield some of the explosive effects. Here, the load generation code would determine which nodes are shielded by tracing rays from the blast epicenter to the edges of the bottom flange and then extending this ray to any intersections on the web or top flange surfaces. Reflected air blast loading would then only be applied to regions of the member that are not shielded from the initial shock wave: the bottom surface of the bottom flanges, the bottom surface of the top flanges nearest the blast, and the upper portion of the web on the side facing the blast, as shown in Fig. 15. The lower part of the girder web facing the explosion is partially shielded from the blast, and in this region side-on overpressure loading would be applied. While the numerical example presented in later in this paper-a wide flange member subjected to an explosion centered on mid-span and mid-height-does not exhibit shielding, the present discussion of shielding is included herein for completeness.

Although shielding is incorporated into the airblast loading code as described above, pressure relief and clearing effects are not accounted for within the current code. Pressure relief occurs after a reflected blast wave reaches a free edge of the reflecting surface. Physically, when an explosive shock wave

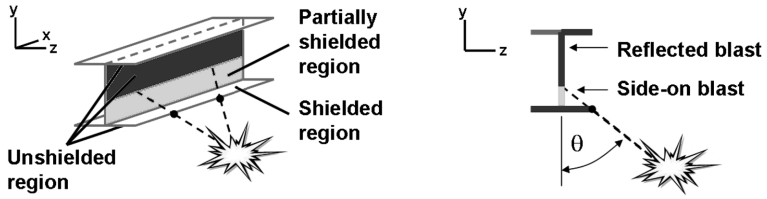

Fig. 15 Schematic of shielding effects included in air blast loading program

impacts a flat surface, pressure is built up by the sudden constraint of flow at the surface, magnifying the blast overpressure here and creating a reflected wave that travels along the structural surface. When the reflected wave reaches a free edge a sudden air flow takes place between high and low pressure regions, creating a rarefaction wave that propagates away from the free edge and back towards the interior of the structural surface. This rarefaction wave acts to relieve the surrounding overpressure from a higher reflected level to a lower stagnation overpressure value. At a point on the surface, this would be modeled by a marked decrease in the air blast overpressure time history after the clearing time, or time when the rarefaction wave reaches the point of interest.

Pressure relief is not included in the air blast loading code because the literature does not provide a universally accepted model of pressure relief. Many sources, including *TM 5-1300* (US Army 1990), Kinney and Graham (1985), and Baker *et al*. (1983), differ in their calculation of the clearing time. Also, while the method for modeling pressure relief in *TM 5-1300* has been used in practice for many years, recent research by Rickman and Murrell (2007) casts doubt onto the accuracy of this approach. Rickman and Murrell (2007) performed several small-scale experiments to measure reflected overpressure values at various points of a rectangular structure subjected to various hemispherical explosions. Their data show that the calculation of clearing time and stagnation pressure provided by *TM 5-1300* (US Army 1990) is inaccurate, and they propose new equations for modeling the stagnation pressure, derived from regression analysis of their experimental data. While these curve fits provide a much better approximation for the reflected air blast loading, they were not incorporated in the developed air blast loading code as these equations were determined for a range of scaled distances from Z = 1.82 to 12.18 m/kg$^{1/3}$, whereas the air blast code was developed for a range of Z = 0.32 to 500 m/kg$^{1/3}$. While the latter portion of the range of scaled distances in the code is not really of engineering significance, the closer range is of extreme interest and in fact both examples presented herein fall in this range.

Another assumption made within the paper is to neglect any loading effects on the far faces of a structural surface. In reality, for a structure such as a wide flange beam, the shock wave from an explosion would almost certainly immediately engulf the structure, imposing positive overpressure on the front faces that would be partially offset by the portion of the shock that wraps around the structure to the back faces. While this is an important physical effect, it is extremely difficult to model with any degree of accuracy. Thus, the loading effects on the far surfaces of structural faces are neglected by the code, inducing a measure of conservatism into model results.

3.5 Code Flow

The developed air blast load generation code essentially works as a preprocessor to a commercial finite element package such as LS-DYNA (Hallquist 2006) or ADINA (ADINA R&D, Inc. 2006).

The code proceeds as shown in Fig. 16. Inputs to the code are the finite element mesh; explosion type,

size, and location; and flag for type of loading. The loading flag corresponds to various sets of parameters available for use in describing the air blast loading including the currently proposed set of equations, the equivalent triangular version of these, the Kingery-Bulmash equations, or the equivalent triangular version of Kingery-Bulmash equations.

There are a few important differences between the developed air blast generation code and the implementation of ConWep in LS-DYNA. Since the air blast code acts as a preprocessor, it is portable to other finite element software packages besides LS-DYNA and it produces loading data that can be analyzed to get an idea of the loads at various locations in a model. However, the implementation of ConWep in LS-DYNA is strictly internal, and only provides the reflected overpressure and arrival time for the node of the structural model first affected by an explosion. The proposed air blast load generation tool can provide loading with air blast parameters derived from open literature sources, whereas ConWep is based on the Kingery-Bulmash equations, which are not openly available. Finally, the air blast loading code includes a shadowing algorithm to determine which components are in direct line-of-sight to an explosion, applying fully reflected loading to these regions and side-on blast loading to partially shielded surfaces.

4. Case studies

Two case studies are presented for investigating the effects of air blast modeling on structural

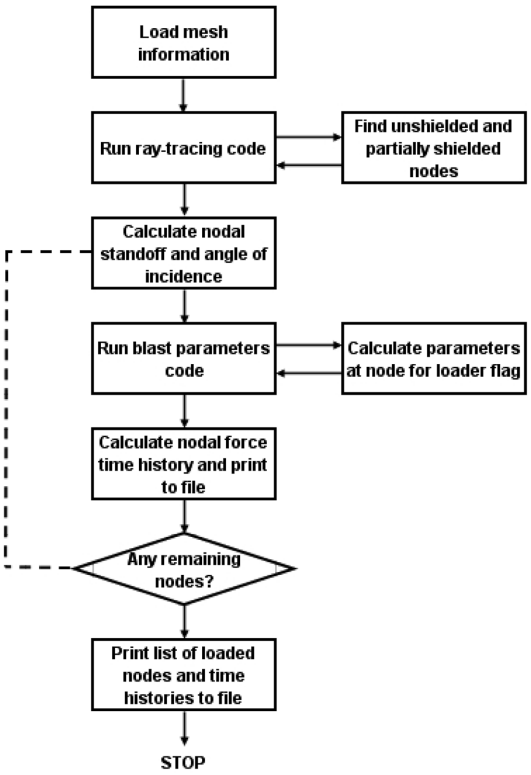

Fig. 16 Air blast loading code flow chart

response. The plate model includes a spatially uniform application of loading (*i.e.*, a plane wave), in order to isolate the effect of different parameter values for a single scaled distance.

The girder model includes the full range of angle of incidence effects as well as a temporally and spatially varying loading.

4.1 Loading

For both of the case studies presented, air blast loading is applied over the structural surfaces using the air blast load generation code. Loads are applied as nodal force time histories within the finite element models. There are four separate cases of loading considered for each structure

1. Currently proposed set of equations – *Current*
2. Equivalent triangular version of *KG* – *Current-Tri*
3. Kingery-Bulmash equations – *KB*
4. Equivalent triangular version of Kingery-Bulmash equations – *KB-Tri*

4.2 Material model

The extreme nature of explosive loading necessitates the inclusion of nonlinear effects for accurate simulations of structures subjected to explosions. This includes not only nonlinear kinematics but also the consideration of rate-dependent material behavior. The commercial finite element package, LS-DYNA, is a transient dynamic nonlinear finite element code with an availability of numerous nonlinear material models (LS-DYNA 2007). Given its wide usage in air blast simulations, LS-DYNA is used as the finite element solver for this research.

A well-known model for rate-dependent material behavior is the Johnson-Cook model (Johnson and Cook 1983, 1985). The Johnson-Cook constitutive relationship is expressed as

$$\sigma_{flow} = [A + B(\varepsilon_{ep})^n][1 + C ln \dot{\varepsilon}^*_{ep}][1 - (T^*)^m], \tag{21}$$

where σ_{flow} is the flow stress, ε_{ep} is the effective plastic strain, $\dot{\varepsilon}^*_{ep} = \dot{\varepsilon}_{ep}/\dot{\varepsilon}_0$ is the dimensionless plastic strain rate, T^* is the homologous temperature, and A, B, n, C, and m are material constants. Note that $\dot{\varepsilon}_0$ is the quasistatic strain rate used in experiments to determine the static strain hardening parameters, B and n.

As part of the present research, a weak form of the heat equation was solved to investigate the spatio-temporally varying temperature field within a representative 12.7 mm thick steel plate component subjected to a thermal loading that was consistent with an open air blast. Based on results from this analysis, heating effects were deemed not to be of concern to the girder and plate problems modeled in this research. Accordingly, ignoring the temperature term gives the simplified version of the Johnson-Cook model used in this research, which is

$$\sigma_{flow} = [A + B(\varepsilon_{ep})^n][1 + C ln \dot{\varepsilon}^*_{ep}]. \tag{22}$$

In this form, the flow stress is the product of a strain hardening term, $[A + B\,(\varepsilon_{ep})^n]$, and a viscoplastic term, $[1 + C ln\ \dot{\varepsilon}^*_{ep}]$.

Johnson-Cook model parameters for a mild steel (SS 141672), as reported by Kajberg and Wikman (2007), are used to model the constitutive behavior for the case studies considered herein. Material

constants used for this steel are $E = 209$ GPa, $\nu = 0.3$, and $\rho = 7{,}850$ kg/m^3 (Andersson *et al*. 2005) for the plate and E = 203 GPa, $\nu = 0.3$, and $\rho = 7{,}850$ kg/m^3 for the girder. The Johnson-Cook parameter values, determined using a split Hopkinson bar test, highspeed photography, and optimization techniques, are reported to be $A = 319$ MPa, $B = 554$ MPa, $C = 3.27 \times 10^{-2}$, $n = 0.135$, $\dot{\varepsilon}_0 = 5.7 \times 10^{-3}$s^{-1} (Kajberg and Wikman 2007).

4.3 Square plate

The first case study involves a square steel plate subjected to a spherical explosion. The plate is 914 mm × 914 mm × 3.18 mm, with fixed boundary conditions on the vertical edges and free boundary conditions along the horizontal edges. A charge of 1.36 kg TNT is centered on the plate, located at a minimum standoff distance of 1.52 m, corresponding to a minimum scaled distance of $Z = 1.37$ kg/m$^{1/3}$. Because of the symmetry in loading and boundary conditions, only 1/4 of the plate is modeled for computational expediency. An overview of the model set-up is shown in Fig. 17.

Explicit time integration is utilized in the solution, along with large strain, large displacement kinematic assumptions. An automatic time-stepping scheme uses the Courant condition to limit step size, producing time steps on the order of 1 μs. The dynamic analysis is carried out to a total solution time of 200 ms, with mass damping (5%) applied after 100 ms in order to yield the final deformed shape of the plate by the end of the analysis. The plate is modeled with Belytschko-Lin-Tsay shell elements with five through-thickness integration points, where a global mesh seed of 4.57 mm is applied. The Belytschko-Lin-Tsay element employs one-point quadrature in the plane of the element and uses empirical parameters to suppress the hourglass deformation modes (Hallquist 2006). Standard viscosity-based hourglass control in LS-DYNA is used, with membrane, bending, and warping hourglass coefficients equal to 0.10. The employed mesh was arrived at by way of a mesh convergence study.

4.4 Girder

The second case study examines the response of a steel wide-flange member to explosive air burst. The girder is a W360 × 122 (W14 × 82) section, 4.57 m long, with simply supported boundary conditions. The investigated air blast scenario involves a spherical explosion of 453.6 kg, centered on the girder and located 4.57 m away from the point at mid-span, mid-height of the girder. This blast scenario corresponds to a minimum scaled distance of $Z = 0.60$ kg/m$^{1/3}$. Fig. 18 illustrates a schematic of the girder model.

The girder is modeled with a combination of elements. Belytschko-Lin-Tsay shell elements, defined along the girder midline geometry with element thickness equal to the girder plate thicknesses,

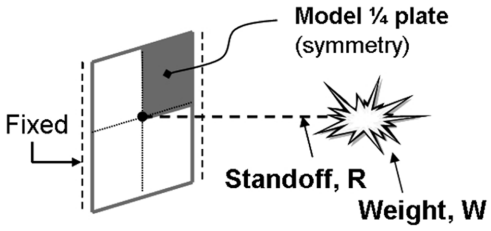

Fig. 17 Plate model set-up

comprise the body of the girder. Cross-sectional distortion at the support locations is suppressed by placing very stiff beam elements along the middle lines of the end crosssections. These beam elements employ the Belytschko-Schwer resultant formulation (Hallquist 2006), and are circular in cross-section with a diameter of 25.4 mm. The material used for the beam elements is perfectly elastic, with $E = 20{,}300$ GPa and $\nu = 0.3$. A mesh seed of 21.4 mm, or 6 elements per flange outstand, applied globally to the model, provides sufficient resolution to capture local deformation effects induced by the explosion, as evidenced by a mesh convergence study.

A dynamic analysis is carried out to a total solution time of 1000 ms. Mass damping (5%) is applied after 500 ms to yield the final deformed shape of the girder by analysis completion. Explicit time integration with automatic time-step calculation is used, producing time steps on the order of 3 μs. To ensure a uniform critical time step size throughout the model, the density of the beam elements is adjusted so that the global model critical time step size is similar for both the shell and beam elements. Accordingly, $\rho = 380\rho_{shell} = 2{,}983 \times 10^3$ kg/m^3, where ρ_{shell} is the density of the shell elements.

5. Results and discussion

5.1 Comparison of overpressure profiles

Air blast overpressure profiles calculated using the four different methods, outlined at the beginning of Section 4, are examined. The main comparisons are made between Kingery-Bulmash versus the proposed parameters developed from Kinney and Graham (1985) and Brode (1977), and between each of these versus their equivalent triangular counterparts. Since the parameter equations draw from different data sets, with only some overlap, it cannot be definitively determined which approach is more correct without access to further explosives test data.

For the loading applied to the plate model, a spherical explosion of $W = 1.36$ kg of TNT, at a standoff of $R = 1.52$ m is employed. Fig. 19 shows the air blast overpressure time histories developed using the four different methods. Parameter values for the different approaches are summarized in Table 3

The largest difference between the loading produced by the proposed equations and the Kingery-Bulmash equations is seen in the load duration, which is not surprising given the amount of scatter in experimental data for air blast duration time that is shown in figures in Baker (1973). When comparing each approach with their triangular equivalents, the most significant difference is seen in the Kingery-Bulmash results since there is such a long tail in the air blast profile produced using this method.

One measure of the differences in air blast overpressure profiles produced by the four approaches is a comparison of their frequency spectrums. Fig. 20 highlights the frequency spectrums, which are

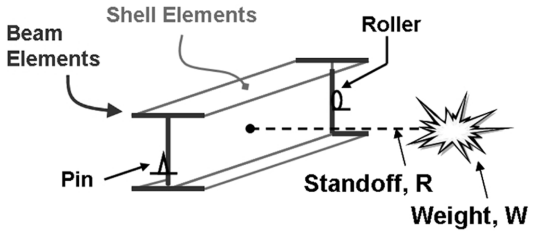

Fig. 18 Girder model set-up

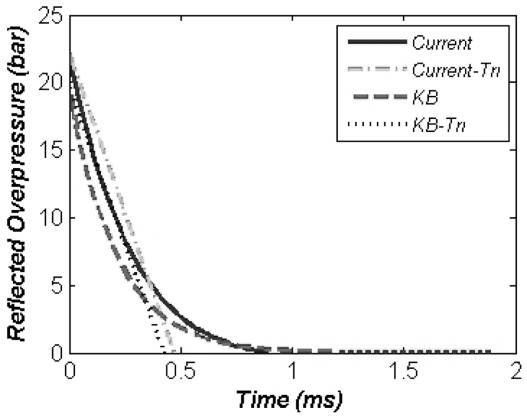

Fig. 19 Comparison of overpressure profiles for $R = 1.52$ m, $W = 1.36$ kg

calculated with fast Fourier transforms (FFT), for the different parameter sets at $R = 1.52$ m and $W = 1.36$ kg. Two universal trends are noteworthy, the first being that the energy in the air blast loading is spread over a wide range of frequencies, and the second being that since the decaying exponential (or equivalent triangle) is not a periodic function, the largest amount of energy is concentrated at zero frequency on the FFT plot.

Closer examination of the frequency content between the specific loading approaches yields a few differences. Since the pulse form for the equivalent triangular approaches varies from their unmodified

Table 3 Air blast parameters for $R = 1.52$ m and $W = 1.36$ kg

Loading	t_a (ms)	t_d (ms)	$t_a + t_d$ (ms)	P_{max} (bar)	I_r (bar-ms)
Current	1.033	0.891	1.924	5.197	22.15
Current-Tri	1.033	0.469	1.502	5.197	22.15
KB	1.072	1.890	2.962	4.124	19.52
KB-Tri	1.072	0.423	1.495	4.124	19.52

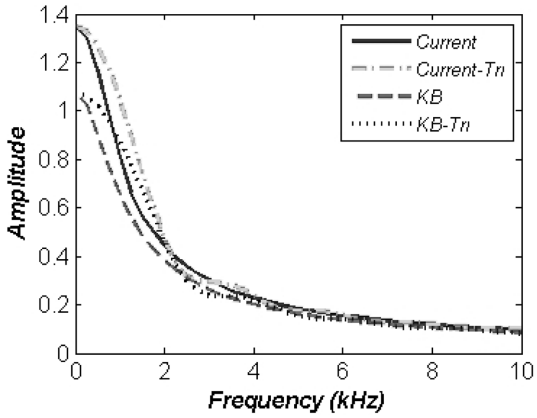

Fig. 20 Comparison of frequency content of air blast loading for $R = 1.52$ m, $W = 1.36$ kg

counterparts, the frequency content of the loading applied to a structure varies slightly. A larger relative difference is seen between the frequency spectrums of the blast profiles for the proposed parameter equations and the Kingery-Bulmash equations. The amplitude of the frequency spectrum of the overpressure loading from the Kingery-Bulmash approach is smaller than that from the proposed equations, a function of the diminished peak overpressure and reflected impulse of the air blast profile from the Kingery-Bulmash equations, as compared with the profile from the proposed equations. However, it is important to note that although the discrepancies in frequency content of overpressure loading produced by the four approaches appear relatively minor within this context, any variation in the frequency content of input loading will lead to differences in simulated structural response time histories.

A detailed comparison is not made between the air blast overpressure profiles that comprise the full spatio-temporal loading for the girder problem. However, the parameter values are reported for the loading at the girder point closest to the explosion (at mid-height and mid-span). At this minimum standoff distance of $R = 4.57$ m, for the charge weight of $W = 453.6$ kg, the parameter values produced by the different loading approaches are shown in Table 4.

5.2 Plate example

Of interest in most explosion simulations is the maximum deformation induced in a structure by a blast. In the plate problem, the peak displacement caused by an air blast occurs at the center of the plate. Accordingly, Fig. 21 shows the transverse displacement results at the center node of the plate for the various loading approaches considered herein. While the results appear similar in the first few cycles of response, they diverge soon after that as the plate starts to plastically deform.

As an illustration of the differences seen in the displacements at a later time after the explosion, transverse displacement results at a specific snapshot in time are examined for the different loading cases. The metric for comparison is the transverse displacement profile along the centerline of the plate at $t = 200$ ms. The profile location is illustrated in Fig. 22 and the resulting plate transverse displacement profiles for the four loading methods are included in Fig. 23.

It is interesting to note that for all of the load approaches except the one using the original Kingery-Bulmash equations, the plate response settles to a permanently deformed configuration that is toward, instead of away from, the explosion epicenter. While this seems counterintuitive, it is not the first time this type of result has been documented. In their investigation of the response of thin circular aluminum plates subjected to a spatially uniform square pulse loading, Bassi, Genna, and Symonds (2002) observed permanent deformation pointed toward the direction of loading. They indicated that for very thin, elastic-perfectly plastic plates with fixed boundary conditions, there exist small ranges of loading parameters for which the plate deforms towards the loading in the early stages of response, and then does not have enough energy left to subsequently snap back away from the loading source. It seems that a similar situation is seen in these results, for a thin plate of a Johnson-Cook material subjected to exponentially

Table 4 Air blast parameters for $R = 4.57$ m and $W = 453.6$ kg

Loading	t_a (ms)	t_d (ms)	$t_a + t_d$ (ms)	P_{max} (bar)	I_r (bar-ms)
Current	1.462	0.816	2.278	57.32	212.34
Current-Tri	1.462	0.540	2.002	57.32	212.34
KB	1.595	3.723	5.318	87.01	201.93
KB-Tri	1.595	0.862	2.457	87.01	201.93

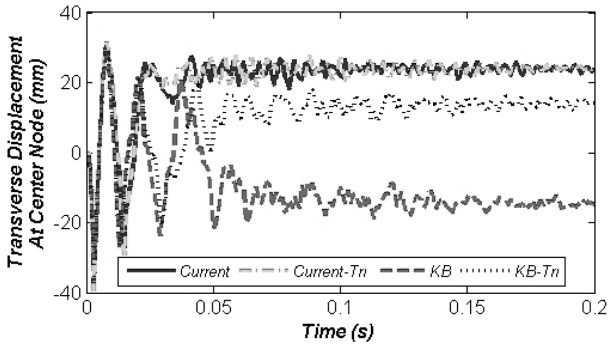

Fig. 21 Comparison of plate transverse displacement at center

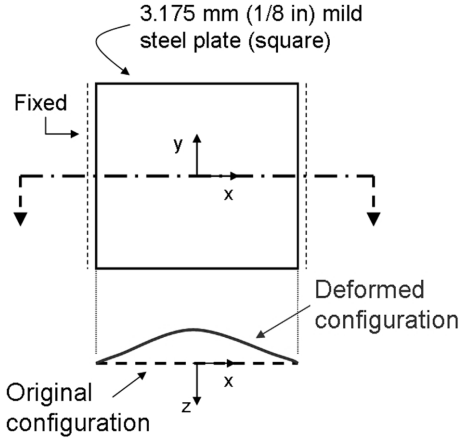

Fig. 22 Schematic of plate center displacement profile

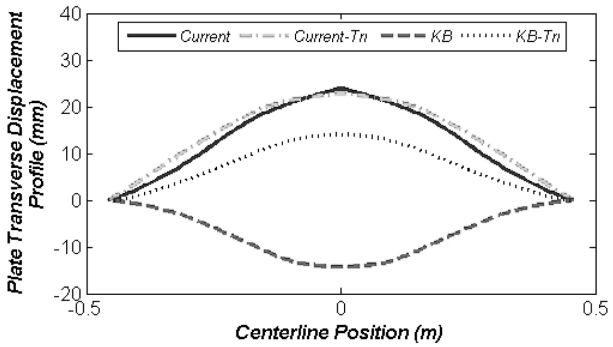

Fig. 23 Comparison of plate center displacement profiles at $t = 200$ ms

decaying and triangular pulse loadings.

Another metric for comparison between the plate responses is a normalized ℓ_2 norm similar to the form in Eq. (11). The error is calculated as

$$\frac{\left\| dz_{Case1}{}^{t} - dz_{Case2}{}^{t} \right\|_2}{\left\| dz_{Case1}{}^{t} \right\|_2} = \frac{\sqrt{\sum_{i=1}^{N} [(dz_{Case1}{}^{t})_i - (dz_{Case2}{}^{t})_i]^2}}{\sqrt{\sum_{i=1}^{N} [(dz_{Case1}{}^{t})_i]^2}} \tag{23}$$

where $(dz_{Case1}{}^{t})_i$ is the transverse displacement at node i along the plate centerline at time $t = 200$ ms for load case number 1, N is the number of nodes along the plate centerline and $(dz_{Case1}{}^{t})_i$ is the transverse displacement at the same time and location for case number 2. Load cases and error results are summarized in Table 5.

The error calculation is greatly affected by the fact that the final deformed configuration of the plate that was loaded with an explosion modeled using the Kingery-Bulmash equations is pointed away from, rather than toward, the blast, in contrast to the other cases. If this profile were flipped so that it faced toward the blast instead, the measured error would change from 3.971 to 0.002 for the second comparison in Table 5 and it would change from 7.195 to 0.480 for the third case. However, it is important to preserve the direction of plate transverse deformation when comparing the actual final deformed shapes since this direction will be important to plate stability under certain structural configurations, such as those experiencing eccentric loading.

5.3 Girder example

In the girder problem, the peak transverse displacements are located at girder mid-height and mid-span. Fig. 24 compares the nodal transverse displacement results at this location on the girder for the different blast loading methods. The transverse displacements produced by the proposed equations developed from Kinney and Graham and Brode match closely with the displacements produced by the corresponding triangular equivalent loading. However, larger differences are seen between the Kingery-Bulmash and equivalent triangular Kingery-Bulmash results, and especially between both sets of Kingery-Bulmash results and the responses induced by the currently proposed air blast loading equations.

Fig. 12 depicts a representative result of simulated girder deformation induced by the explosion. This contour plot of averaged accumulated effective plastic strain represents the girder response at $t = 1$ s for the equivalent triangular Kingery-Bulmash loading. Two main features are noteworthy, the permanent set in the web away from the blast, and the deformation within the compression flanges nearest the detonation epicenter.

Further examination of the flange vertical displacement is warranted since the magnitude and location of localized deformations oftentimes greatly affects the global capacity of a structural member within a system. In Fig. 25, the y-displacements at each node along the top flange edge nearest the blast are compared for the different loading cases at $t = 1$ s, long after the plastic strains have stopped changing in this region. These results take the form of displacement profiles along the girder top flange edge, which clearly show regions of localized deformation.

.

Table 5 Relative error between plate transverse displacement profiles at $t = 200$ ms

Case 1	Case 2	Error, $\frac{\left\| dz_{Case1}{}^{t} - dz_{Case2}{}^{t} \right\|_2}{\left\| dz_{Case1}{}^{t} \right\|_2}$
Current	*Current-Tri*	0.013
KB	*KB-Tri*	3.971
Current	*KB*	7.195

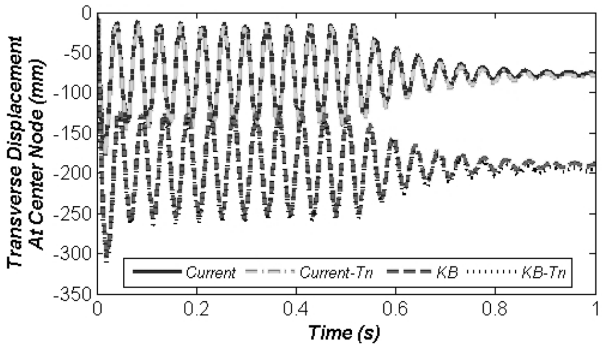

Fig. 24 Comparison of girder transverse displacement at mid-height, mid-span

A quantitative comparison of the displacement profiles can be made with an ℓ_2 norm, or

$$\|dy\|_{\infty} = \max_{i=1}^{N} (\mathrm{dy}_{\mathrm{i}}^{\mathrm{t}}), \tag{24}$$

where dy_i^t corresponds to the y-displacement at the nodes along the top flange edge nearest to the blast at time t = 1 s, and N is the number of nodes. The peak vertical displacements are 17.6, 25.3, 7.0, and 8.1 mm for the Kingery-Bulmash equations, the Kingery-Bulmash triangular equivalent, the proposed equations developed from Kinney and Graham and Brode, and the triangular equivalent of the proposed equations, respectively. The peak flange displacement occurs near midspan for all loading methods, in spite of their relative similarities. Similar to the plate case study, the four different load approaches produce significantly different results. In terms of relative comparisons, the peak displacements are closer in magnitude for the equivalent triangular pulse loading, as compared with their parent parameter equations, than they are between the Kingery-Bulmash and the proposed parameter cases.

The flange displacement profile is more exaggerated for the cases with Kingery-Bulmash types of loading than those loaded by a variant of the proposed parameters from Kinney and Graham and Brode. At first glance, it would seem that this is purely due to the substantial difference in predicted reflected impulse between these loading approaches. However, parameter studies on the research presented herein, and numerous sources in the literature (Mays and Smith 1995, Smith and Hetherington 1994, Baker *et al*. 1983), show that there is a strong interrelationship between pressure and impulse, and so

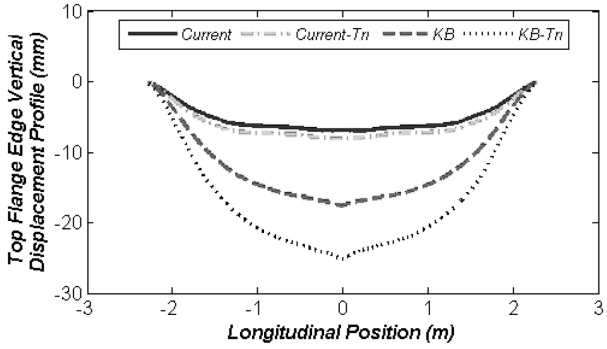

Fig. 25 Comparison of girder flange edge displacement profile at t = 1 *s*

the difference in structural response cannot be traced to either of these parameters acting in isolation. In fact these results clearly show that duration time is also important to response, since there is such a wide range between the deformation caused by the Kingery-Bulmash loading as compared to its triangular equivalent. While discussing differences, it is important to note that the Kingery-Bulmash loading and the proposed set of parameter equations emanated from different empirical data sets for open air blast tests. It is expected that variations within these tests plays a significant role in precipitating some of the differences highlighted earlier.

6. Conclusions

Structural vulnerability to acts of terrorism has received increasing attention in the past few years. A first step toward accurate simulation of structural response to different explosion scenarios is to establish suitable models of loading. To this end, this research presents a complete set of parameter equations to describe external air blast loading for a structure, based on open literature sources (Kinney and Graham 1985, Brode 1977). The proposed air blast parameters are notable in that they are drawn from data available in the open literature and that they are in equation, rather than graphical form. These parameters, together with alternative parameter methods (the Kingery-Bulmash equations, and equivalent triangular pulses), have been implemented within an air blast load generation code written for this research. This code improves upon other codes in its inclusion of a shadowing algorithm for determination of unshielded and partially shielded structural surfaces, and its application of side-on, rather than fully reflected, blast to surfaces partially shielded from explosive air burst. Additionally, given its open literature sources, all assumptions and limitations within the proposed approach are available for critical review by the analyst/designer.

The proposed blast load generation code is used to provide loading representing each set of parameters in finite element simulations of a steel plate and a W14 × 82 girder subjected to an explosive air burst. Results obtained by coupling the currently developed air blast load generation code with LS-DYNA illustrate that small changes in blast loading parameter definition can have a significant effect on structural response time histories. Since small details have such a large effect on structural response for air blast phenomena, there is a clear need for further research to better assess the unavoidable uncertainty that is inherent in air blast loading.

Acknowledgment

This material is based upon work supported under a National Science Foundation Graduate Research Fellowship. Any opinions, findings, conclusions or recommendations expressed in this publication are those of the author and do not necessarily reflect the views of the National Science Foundation.

References

ADINA R&D, Inc. (2006), *ADINA Theory and modeling guide*, Watertown, MA.

Andersson, R., Syk, M. and Magnusson, C. (2005), "The development of high strain rate equations for stainless steels", *J. Mater. Eng. Perform.*, **14**(5), 553-562.

Baker, W.E. (1973), *Explosions in Air*, University of Texas Press, Austin.
Baker, W.E., Cox, P., Westine, P.S., Kulesz, J.J. and Strehlow, R.A. (1983), *Explosion hazards and evaluation*, Elsevier, New York.
Bassi, A., Genna, F. and Symonds, P. (2002), "Anomalous elastic-plastic responses to short pulse loading of circular plates", *Int. J. Impact. Eng*., **28**, 65-91.
Baylot, J.T. and Rickman, D.D. (2007), "Uncertainties in blast loads on structures", *Proceedings of ASCE Structures Congress*.
Beshara, F.B.A. (1994), "Modelling of blast loading on aboveground structures-I, general phenomenology and external blast", *Compos. Struct*., **51**(5), 585-596.
Bleakney, W., White, D. and Griffith, W. (1950), "Measurements of diffraction of shock waves and resulting loading of structures", *J. Appl. Mech. T-ASME,* **17**(4), 439-445.
Bogosian, D.D., Ferritto, J. and Shi, Y. (2002), "Measuring uncertainty and conservatism in simplified blast models", *30th DoD Explosives Safety Seminar Proceedings,* Department of Defense Explosives Safety Board, Atlanta, GA.
Borenstein, E. and Benaroya, H. (2009), "Sensitivity analysis of blast loading parameters and their trends as uncertainty increases.", *J. Sound. Vib.*, **321**(3-5), 762-785.
Brode, H.L. (1977), *Quick estimates of peak overpressure from two simultaneous blast waves*, Tech. Rep. DNA4503T, Defense Nuclear Agency, Aberdeen Proving Ground, MD.
Chock, J.M. and Kapania, R.K. (2001), "Review of two methods for calculating explosive air blast", *Shock. Vib.*, **33**(2), 91-102.
Corley, W.G. (2004), "Lessons learned on improving resistance of buildings to terrorist attacks", *J. Perform. Constr. Fac.*, **18**(2), 68-78.
Florek, J. and Benaroya, H. (2005), "Pulse-pressure loading effects on aviation and general engineering structures-review", *J. Sound. Vib.*, **284**(1-2), 421-453.
Hallquist, J.O. (2006), *LS-DYNA Theory Manual,* Version 971, Livermore Software Technology Corporation, Livermore, CA.
Hyde, D. (1992), *ConWep-Application of TM5-855-1*, Structural Mechanics Division, Structures Laboratory, USAE Waterways Experiment Station, Vicksburg, MS.
Johnson, G.R. and Cook, W.H. (1983), "A constitutive model and data for metals subjected to large strains, high strain rates and high temperatures", *Proceedings of 7th International Symposium on Ballistics*, The Hague, The Netherlands, 541-547.
Johnson, G.R. and Cook, W.H. (1985), "Fracture characteristics of three metals subjected to various strains, strain rates, temperatures and pressures", *Eng. Fract. Mech*., **21**(1), 31-48.
Kajberg, J. and Wikman, B. (2007), "Viscoplastic parameter estimation by high strain-rate experiments and inverse modelling-speckle measurements and high-speed photography", *Inter. J. Solids. Struct.*, **44**(1), 145-164.
Kingery, C.N. and Bulmash, G. (1984), *Airblast parameters from TNT spherical air burst and hemispherical surface burst*, Tech. Rep. ARBRL-TR-02555, Armament Research and Development Center, Ballistic Research Laboratory, Aberdeen Proving Ground, MD.
Kinney, G.F. and Graham, K.J. (1985), *Explosive Shocks in Air*, Springer-Verlag, New York, 2nd edn.
LS-DYNA (2007), *LS-DYNA Keyword User's Manual, Version 971*, *Vols. 1-2*, Livermore Software Technology Corporation, Livermore, CA.
Mays, G.C. and Smith, P.D. (1995), *Blast Effects on Buildings*, Thomas Telford Service Ltd., London.
Randers-Pehrson, G. and Bannister, K.A. (1997), *Airblast loading model for DYNA2D and DYNA3D*, Tech. Rep. ARL-TR-1310, Army Research Laboratory, Aberdeen Proving Ground, MD.
Rickman, D.D. and Murrell, D.W. (2007), "Development of an improved methodology for predicting airblast pressure relief on a directly loaded wall", *J. Press. Vess. T-ASME*, **129**, 195-204.
Santiago, J. and Bhattacharya, S. (1991), "Sensitivity of plate response calculations to blast load definition", *Compos. Struct*., **40**(2), 375-392.
Smith, P.D. and Hetherington, J.G. (1994), *Blast and ballistic loading of structures*, Butterworth-Heinemenn Ltd., London.
US Army, U.A.F., US Navy (1990), *Structures to resist the effects of accidental explosions*, Tech. Rep. TM 5-1300/NAVFAC P-397/AFR 88-22.

CC